Hindawi Publishing Corporation
Journal of Renewable Energy
Volume 2013, Article ID 190573, 8 pages
http://dx.doi.org/10.1155/2013/190573

Research Article

Evaluation of Harmonic Content from a Tap Transformer Based Grid Connection System for Wind Power

S. Apelfröjd and S. Eriksson

Swedish Center for Renewable Electric Energy Conversion, Division for Electricity, Uppsala University, P.O. Box 534, 751 21 Uppsala, Sweden

Correspondence should be addressed to S. Apelfröjd; senad.apelfrojd@angstrom.uu.se

Received 30 November 2012; Revised 6 May 2013; Accepted 25 June 2013

Academic Editor: Joydeep Mitra

Simulations done in MATLAB/Simulink together with experiments conducted at the Ångströms laboratory are used to evaluate and discuss the total harmonic distortion (THD) and total demand distortion (TDD) of a tap transformer based grid connection system. The grid connection topology can be used with different turbine and generator topologies and is here applied on a vertical axis wind turbine (VAWT) with a permanent magnet synchronous generator (PMSG) and its operational scheme. The full variable-speed wind conversion system consists of a diode rectifier, DC link, IGBT inverter, LCL-filter, and tap transformer. The full variable-speed operation is enabled by the use of the different step-up ratios of the tap transformer. In the laboratory study, a full experimental setup of the system was used, a clone of the on-site PMSG driven by a motor was used, and the grid was replaced with a resistive load. With a resistive load, grid harmonics and possible unbalances are removed. The results show a TDD and THD below 5% for the full operating range and harmonic values within the limits set up by IEEE-519. Furthermore, a change in tap, going to a lower step-up ratio, results in a reduction in both THD and TDD for the same output power.

1. Introduction

Installed wind power on the utility grid is rapidly increasing [1]. The injection of wind power into the electric grid will affect the voltage quality. As the voltage and power quality must be within certain limits to not cause problems on the utility grid, the impact of different grid connection schemes needs to be assessed prior to installation. Several authors bring up the importance of this subject as more and more distributed and intermittent power is introduced into the grid [2–5]. Power electronics play an important role in distributed generation and in integration of renewable energy sources into the grid [2]. This paper mainly focuses on wind power where there are two strong arguments for the use of full power electronic conversion systems. First, the ability to control the rotational speed almost freely giving the benefit of optimal energy absorption, reduced loads, gearless turbines, and reduced noise at low wind speeds. Second, the power electronics give the wind turbine the ability to be an active component in the power system [6]. This allows for control of active and reactive power flow and the ability to strengthen weak grids. An evaluation of today's most commonly used power conversion topologies for wind power can be found in [7, 8].

A three bladed vertical axis wind turbine (VAWT) with a direct driven permanent magnet synchronous generator (PMSG) has been developed and built at Uppsala University. The idea behind the innovative concept is to reduce the number of moving parts to achieve a robust and cost-effective design. The variable speed vertical axis wind turbine is passively stall regulated and does not require any pitch mechanism. The direct driven generator eliminates the need for a gearbox and is, together with the rest of the electric components, placed at ground level. This paper contributes to the research done on the 12 kW VAWT prototype at Uppsala University [9–13]. The prototype turbine can be seen in Figure 1, and some of its design parameters are shown in Table 1. The electrical system for the grid connection of the turbine has been assembled in the laboratory at the Division for Electricity at Uppsala University. The work presented in this paper aims to evaluate the total harmonic distortion (THD) and total demand distortion (TDD) of the system.

Table 1: Turbine parameters.

Rated rotational speed (rpm)	127
Rated wind speed (m/s)	12
Swept area (m^2)	30
Hub height (m)	6
Turbine radius (m)	3

Figure 1: 12 kW vertical axis wind turbine designed and constructed at Uppsala University.

In the experimental setup, a clone of the on-site PMSG driven by an induction motor is used and the grid is replaced with a resistive load. The use of a resistive load will eliminate grid effects such as unbalances and harmonics. The results from the experiments are compared with simulations done in MATLAB/Simulink. The tap transformer based grid connection system topology can be adapted and used for other renewables where a full frequency conversion is needed.

2. System Design and Theory

The system in this paper is evaluated based on the THD and the TDD of the current. The total harmonic content in the current, THD_I, is calculated using (1) in accordance with IEEE-519 [14]. Consider the following:

$$\mathrm{THD}_I = \left[\frac{\sqrt{\sum_{h=2}^{H} I_h^2}}{I_1}\right] 100\%, \tag{1}$$

where I_h is the amplitude of the hth harmonic and I_1 the amplitude of the fundamental. The amplitudes of the current harmonics are derived with the use of the fast Fourier transform (FFT) with a flat top window. The total demand distortion of the current waveform, TDD_I, is given in (2)

$$\mathrm{TDD}_I = \left[\frac{\sqrt{\sum_{h=2}^{H} I_h^2}}{I_L}\right] 100\%, \tag{2}$$

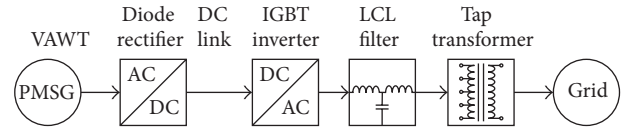

Figure 2: System block diagram.

where I_L is the fundamental maximum demand load current. The total demand distortion can often be difficult to apply as it can be difficult to determine the location of the point of common coupling (PCC). For the study in this paper, we assume the maximum demand current to be the nominal current of the system at rated load. This gives a worst case scenario in respect of TDD. The current harmonic distortion limits for general distribution systems given in IEEE-519 are shown in Table 2 where I_{sc} is the maximum short-circuit current at the PCC.

An illustration of the system topology is shown in Figure 2. In the following text, each block in Figure 2, from left to right, is described.

The vertical axis wind turbine is of the fixed pitch H-rotor type with three blades. The amount of power, P_t, that can be extracted from the turbine is given by (3)

$$P_t = \frac{1}{2}\rho A C p\,(\lambda)\, v^3, \tag{3}$$

where ρ is the air density, A is the area swept by the turbine, Cp is the power coefficient, and v is the wind speed. The power coefficient is a function of tip speed ratio (λ) and represents the aerodynamic efficiency of the turbine. The tip speed ratio is defined in (4)

$$\lambda = \frac{\omega_t R}{v}, \tag{4}$$

where ω_t is the turbine rotational speed and R is the turbine radius. The $Cp - \lambda$ characteristics and the designed control strategy for the turbine can be found in [10]. The system is run at an optimal Cp for wind speeds of 4 m/s to 10 m/s. This is done by the use of a maximum power point tracking (MPPT) algorithm. In this paper, the MPPT algorithm is assumed to keep the turbine at optimal Cp in this region. In the range of 10 m/s to 12 m/s, the turbine is kept at a fixed rotational speed. The rotational speed will still have small variations in this region due to controller limitations and current variations. However, the variations will be small, and it can still be seen as fixed speed operation. For all wind speeds above 12 m/s until cutout, the turbine is run at nominal power. This differs from the designed control strategy where the turbine would have been kept at fixed rotation speed until the cutout wind speed of 15 m/s.

The voltage from the direct driven permanent magnet synchronous generators is rectified via a passive diode rectifier, and smoothened on the DC link with a capacitor bank. The voltage on the DC link varies greatly due to the variable speed operation and passive rectification. The variations in the DC voltage will be managed by changing the modulation index of the inverter and using different

Table 2: Current distortion limits for general distribution systems (120 V through 69 kV).

	Maximum harmonic current distortion in percent of I_L Individual harmonic order (odd harmonics)					
I_{sc}/I_L	<11	$11 \le h < 17$	$17 \le h < 23$	$23 \le h < 35$	$35 \le h$	TDD
<20	4.0	2.0	1.5	0.6	0.3	5.0
20–50	7.0	3.5	2.5	1.0	0.5	8.0
50–100	10.0	4.5	4.0	1.5	0.7	12.0
100–1000	12.0	5.5	5.0	2.0	1.0	15.0
>1000	15.0	7.0	6.0	2.5	1.4	20.0

Even harmonics are limited to 25% of the odd harmonic limits above.

Table 3: Filter and tap transformer values.

Tap	1	2	3
Step-up ratio	7	4	3
Input voltage Ph-Ph rms (V)	57	100	133
Output voltage Ph-Ph rms (V)	400	400	400
Filter side coil L_{t1} (μH)	28	51	88
Grid side coil L_{t2} (μH)	64	64	64
Magnetization resistance R_m ($k\Omega$)	1.8	1.8	1.8
Magnetization inductance L_m (H)	1.6	1.6	1.6
Inverter side filter coil (μH)	400	400	400
Tap transformer side filter coil (μH)	150	150	150
Filter capacitor (μF)	100	100	100

Table 4: Relevant generator parameters.

Per phase inductance (mH)	2.6
Per phase resistance (Ω)	0.16
Nominal rms phase voltage (V)	161
Nominal electrical frequency (Hz)	33.9

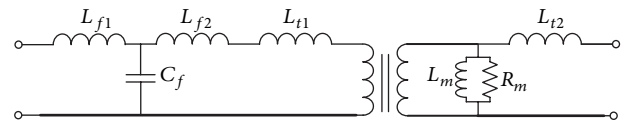

Figure 3: One phase equivalent circuit of the LCL filter and one tap of the tap transformer.

taps on the transformer. In more conventional systems, DC voltage is usually handled with a DC/DC converter or an active rectifier. A tap transformer with four taps has been chosen for this system. However, the tap with the lowest step-up ratio is not used in this study. The four taps of the transformer have step-up ratios of 2, 3, 4, and 7, respectively. The tap transformer has a star-delta configuration with the delta side connected to the load. An IGBT based voltage source inverter (VSI), controlled with sinusoidal pulse width modulation (SPWM), is used to convert the DC voltage to the desired three phase 50 Hz AC voltage. The inverter output voltage is filtered through an LCL filter and the tap transformer before it reaches the load. The use of an LCL filter is suggested in several papers [15–19]. The LCL filter offers a cost effective solution with good filtering properties. The one phase equivalent circuit of the LCL filter and tap transformer can be seen in Figure 3 with the corresponding component values in Table 3. The design of the filter and evaluation of the filter parameters are done in [20]. The filter is designed to filter out high order frequencies and does not affect the fundamental. In the design, the filter resonance frequency was placed roughly at 1 kHz as not to affect low order frequencies and harmonics but still has good damping at the switching frequency.

2.1. Tap Transformer Operation. The system is operated using all three taps, and the tap change is done as soon as a tap with a higher step-up ratio is available, with some hysteresis implemented. The hysteresis will not affect the distortion for a given transformer tap and wind speed. The strategy for tap changes is therefore as follows: in winds from 4 m/s until 7 m/s tap 1 is used, from 7 m/s until 9 m/s tap 2 is used, and for the rest of the wind speeds tap 3 is used. The possible distortion during a tap change is not examined in this paper as it will be very dependent on how the tap change is done and will not affect the distortion of the system for a given transformer tap and wind speed.

3. Experimental Setup

The topology of the system is illustrated in Figure 2. In the following subsections, each block in Figure 2 as it is implemented in the experimental setup, from left to right, will be described.

The generator, seen in Figure 4, is identical to the direct driven generator installed in the 12 kW VAWT prototype. The generator has a round rotor and is star connected with the neutral not connected. Relevant electric generator parameters are presented in Table 4. Previous work on this generator can be found in [9]. In the experiment, the generator is driven by an induction motor.

The AC/DC conversion in Figure 2 consists of a diode rectifier and a capacitor bank. The generator phase currents are rectified using semikron SKKD 100/12 rectifier modules rated at 1.2 kV and 100 A. The rectified current charges a capacitor bank consisting of 3 RIFA 6000 μF 450 VDC capacitors, connected so that the total capacitance is 18 mF. The IGBT modules used in the inverter are of the type SEMiX252GB126HDs with Skyper 32R drivers, see Figure 5.

Figure 4: Permanent magnet synchronous generators used in the experimental setup.

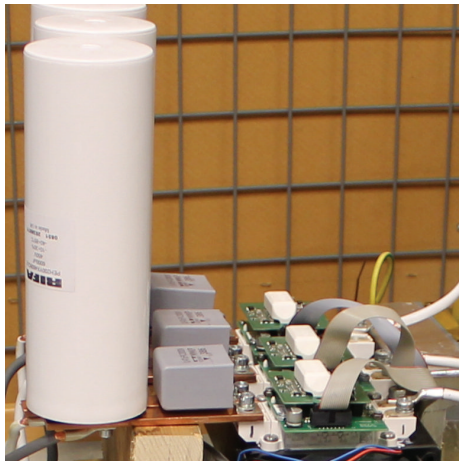

Figure 5: IGBT based voltage source inverter used in the experimental setup and the DC bank capacitors.

The tap transformer, seen in Figure 6, is delta star connected with the delta side connected to the resistive load. A schematic figure of the filter and inverter is shown in Figure 7 with the single phase equivalent circuit shown in Figure 3. The transformer and filter parameters are given in Table 3. Previous work done on the tap transformer and LCL filter can be found in [20].

The resistive load consists of modified electric heaters with a maximum power rating of 2 kW, respectively. The resistors were connected to produce eight different loads within the operating range of the system resulting in up to six different loads per tap as not all loads are applicable on all taps for the given turbine operation. The corresponding wind speeds and turbine rotational speeds for each tap are given in Table 5.

Table 5: Wind speeds and corresponding turbine rotational speed covered in the experiments and simulations.

Tap	Wind speed (m/s)	Turbine rotational speed (rpm)
1	5.9, 7.4, 8.2	62, 78, 87
2	6.7, 7.6, 8.4, 11.2, 11.5, 11.9, 12.2	71, 80, 89, 127, 127, 127, 127
3	10.4, 11.2, 11.5, 12.0	127, 127, 127, 127

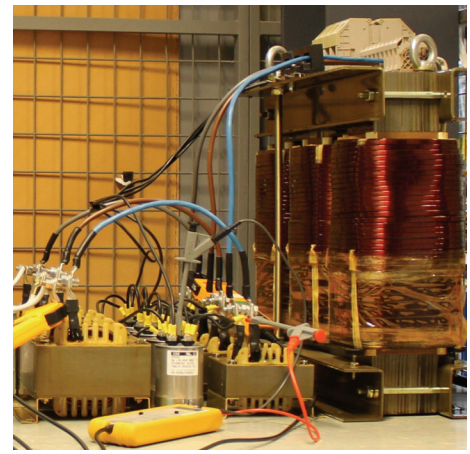

Figure 6: LCL filter to the left and tap transformer to the right.

4. Simulation

The system described in Section 2 was modeled in MATLAB/Simulink using the built in power systems blocks. The model is shown in Figure 7. A simple representation of the PMSG was chosen as we only need to include the frequency from the machine. By combining (3) and the control strategy for the turbine, a relation between power output and wind speed is derived. The simulation is then run so that the power drawn from the DC link corresponds to the correct wind speed and DC link voltage. The power referred to in (3) is assumed to be available on the DC link. Both the amplitude modulation of the inverter and the resistance of the load are varied to fit the control strategy and keep the load voltage at a constant 400 V Ph-Ph. The inverter is run at a switching frequency of 6 kHz, and the PWM pulses are generated using a phase locked loop (PPL) and dq-controller with a 50 Hz sinusoidal reference signal. The simulations are done for two different cases, corresponding to two different transformer models.

Case 1. Each tap of the tap transformer is represented by a linear star-delta connected transformer. A saturation model of the transformer core is not used. The losses and transformer core effects on the system are reflected by the magnetizing impedance, R_m and L_m.

Case 2. The tap transformer is modeled using a linear star-delta transformer representing each tap. A simple saturation model for the transformer core without hysteresis is implemented in accordance with [21, 22], where the saturation effects are described by an arctan function with the saturation

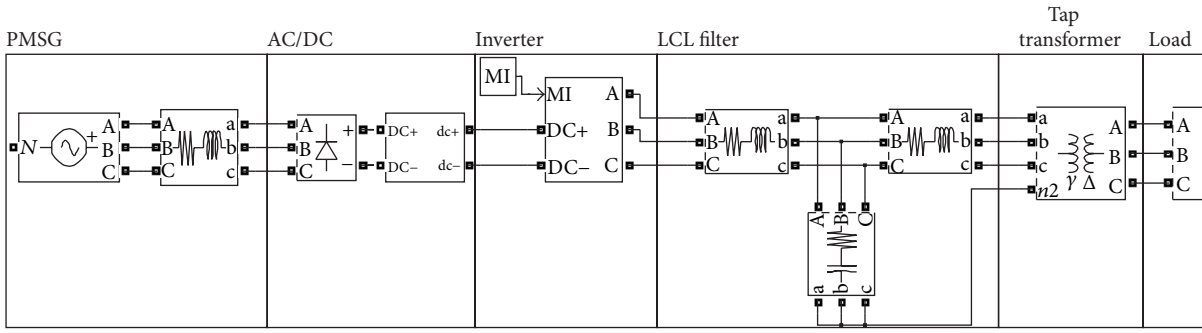

Figure 7: Simulink model of the tap transformer based grid connection system. The generator is to the left followed by the passive diode rectifier, IGBT based inverter, LCL-filter, and one tap of the tap transformer connected to a resistive load.

limits at 120% of the nominal voltage and nominal magnetizing current, derived from the magnetizing impedance. The core flux, Φ_{core}, as a function of magnetizing current, I_{mag}, used in this model is shown in (5) where A_o and A_1 are shape constants. The function is used for positive currents and then mirrored symmetrically to the negative quadrant. All of the transformer losses are expressed by the magnetizing resistance, R_m

$$\Phi_{\text{core}}\left(I_{\text{mag}}\right) = A_o \arctan\left(A_1 I_{\text{mag}}\right). \tag{5}$$

The harmonic content of the current across the load is evaluated in both cases.

5. Experiments

The quality of the filtered output was determined by measuring the load current as voltage over known resistors during operation. Each phase voltage and current was sampled at 150 kHz with a PicoScope 4424. The system was run with different generator rotational speeds, taps, and modulation index from operational data collected from the simulations. This means that the simulations were run for the fixed resistive loads available in the experimental setup and the generator, and inverter operational data was collected and used in the experiment for the corresponding load. The same inverter control scheme, with an internally generated PLL reference, was used in the experimental setup as in the simulations. The control of the inverter was implemented on the built-in FPGA of the NI-cRIO9074 unit and executed with a NI9401 digital output module.

A limiting factor for the experiments on the tap with highest step-up ratio was the current. The experimental system has a current limit of 80 A per phase. This limits the power per phase on transformer tap 1 to roughly 2.6 kW, whereas the other taps were limited by their inability to produce a sufficiently high AC voltage at low DC voltage. A limitation for all taps was the discrete resistance values that only allowed for a few measurement points in the operational range.

6. Results and Discussion

The experimental results are shown in Figure 8. The two vertical lines, in both Figures 8(a) and 8(b), correspond to one-third and two-thirds of the nominal power. The system THD as a function of wind speed is presented in Figure 8(a). The system THD is highest at low wind speeds and decreases with increasing wind speed. We can see a significant drop in the total harmonic distortion when we make a tap change to a lower step-up ratio. The effect is greater when we have a larger change in the step-up ratio. The change from tap 1 to tap 2 has a greater reduction than the step from tap 2 to tap 3, see Figure 8(a). This effect was expected, as we utilize a larger part of the inverter side transformer winding at low step-up ratios.

The system TDD as a function of wind speed is presented in Figure 8(b). The TDD is lowest at low wind speed and increases with higher wind speeds. As we move up in wind speed, the TDD goes up mostly due to the increase in output current from the system. Here we also see the same trends during tap change as with the THD, which is a reduction when operating on a lower step-up ratio. Note that the system has its best TDD at the same time as the THD is at its highest value. The THD and TDD are assumed to be roughly constant for the wind speeds from 12 m/s until 15 m/s. This is due to that the turbine operates at a fixed power within this region. There will still be small DC voltage variations due to the speed reduction during stall, but this is believed to have a very small effect on the THD and TDD. The system TDD is well within the limits set in IEEE-519 for the full operating range.

The reduction in distortion at a tap change follows from the shift in the operating point of the system. When we change the tap ratio, we also move the rest of the system to a new operating point. For a given wind speed, the rotational speed of the turbine will be the same after a change giving the same output voltage due to the direct drive. This means that the modulation of the inverter will have to be increased to fit the new lower step-up ratio. As the power from the turbine is constant at a given wind speed, this also results in a lower current due to the increase in voltage.

The FFT normalized to percentages of the fundamental for the simulated and experimental currents at nominal load is shown in Figure 9. This figure gives an overview of the harmonics present in the output from the system. We can see the typical switching frequency harmonics in

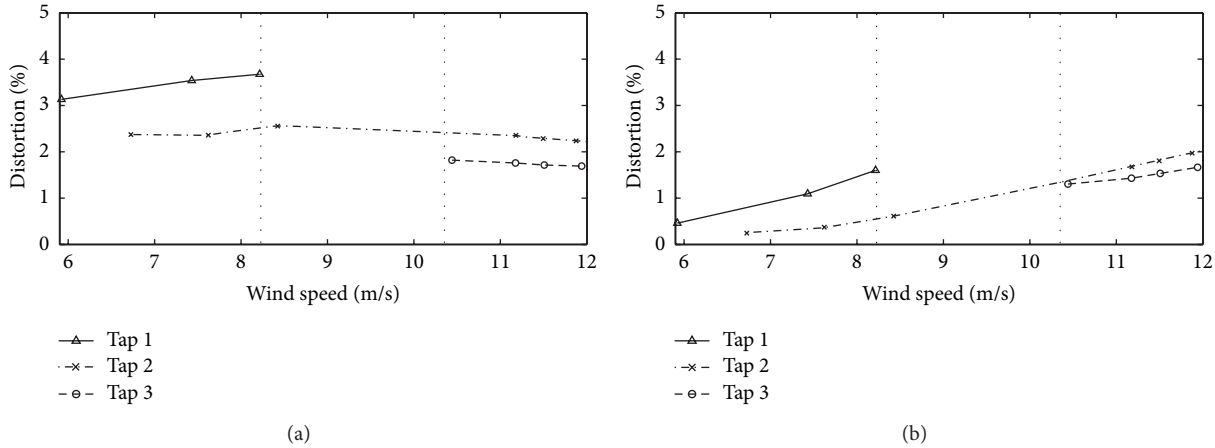

Figure 8: Results from the experiments for all three taps on the tap transformer (a) THD (b) TDD. The vertical lines in the two figures correspond to one-third and two-thirds of the nominal power from the turbine. We can see an improvement in THD as we go up in power and an improvement in both THD and TDD as we go up in tap.

the high frequency range. The experimental filter damping is somewhat lower than for the simulated system. This is probably since the inductors in the experimental setup are optimized for 50 Hz operation and have limitations in the higher frequency range.

We also have a significant amount of low order harmonics present in the experimental data. In this region, $h < 11$, the simulations of Cases 1 and 2 have a clear difference. The lower order harmonics in the Case 2 simulation, where we have a basic transformer core saturation model implemented, have a higher amplitude than in Case 1. The low order harmonics in the experimental data are believed to be due to the magnetization of the transformer, systems imbalances, and some variations in the DC link voltage. During grid connection, the magnetization of the transformer can be supplied by the inverter and the magnetization currents will have less impact on the harmonic content of the output current. In this experiment, there is no set voltage on the connection point so the magnetization of the transformer can not be separated from the output.

The measured maximum value of the harmonics within the ranges specified by IEEE-519 and the total TDD at nominal load are shown in Table 6. The measured value of the TDD meets the demands for all cases in Table 2, but due to the presence of the high order harmonics, the system does not meet the requirements for the case of $I_{sc}/I_L < 20$. However, this case of $I_{sc}/I_L < 20$ represents a very weak grid.

The voltage waveform across the resistive load from the experiments at nominal load is shown in Figure 10. Figure 10(a) shows the line to neutral voltage across the load at the lowest THD from the results shown in Figure 8. Here we can visually determine that there are some low order harmonics left in the output, and we can also see a small presence of the switching frequency. Figure 10(b) shows the highest THD from the results shown in Figure 8(a). Here we can see more distortion, but the voltage still has a good shape.

The results presented here show that the system is operated within the THD and TDD limits of IEEE-519 [14],

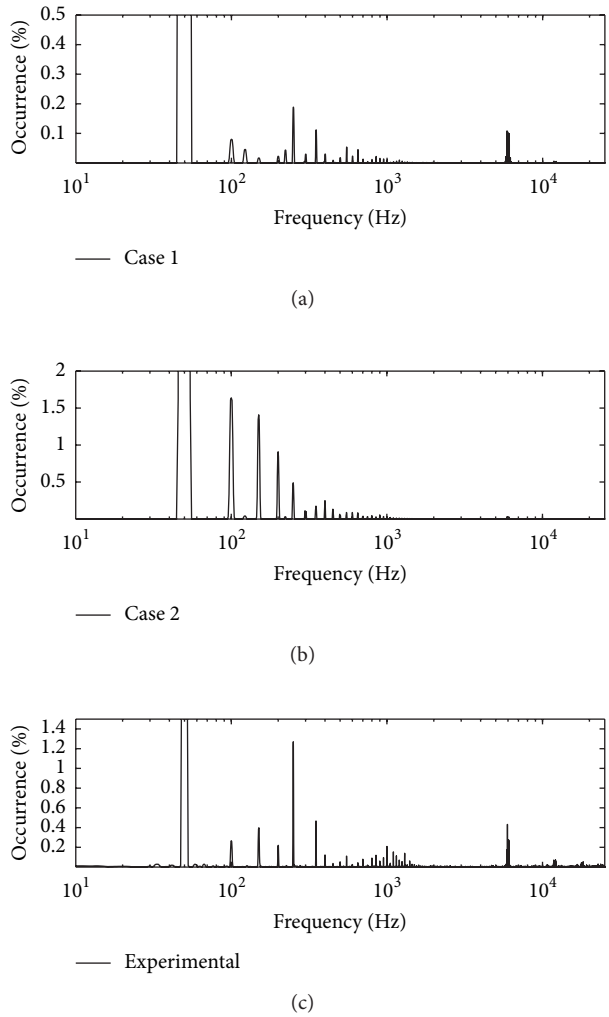

Figure 9: FFT of phase A at nominal power. (a) Case 1. (b) Case 2. (c) Experimental. We see that there are more low order harmonics in the Case 2 simulation than in Case 1. The occurrence is presented as percent of the first harmonic, that is, $(I_h/I_1)\%$.

Table 6: Maximum harmonic current distortion in percent of I_L for nominal power.

	<11	$11 \leq h < 17$	$17 \leq h < 23$	$23 \leq h < 35$	$35 \leq h$	Total THD
Simulated Case 1	0.18	0.05	0.01	0.01	0.1	0.43
Simulated Case 2	0.8	0.05	0.04	0.01	0.02	1.52
Measured	1.31	0.12	0.2	0.13	0.41	1.69

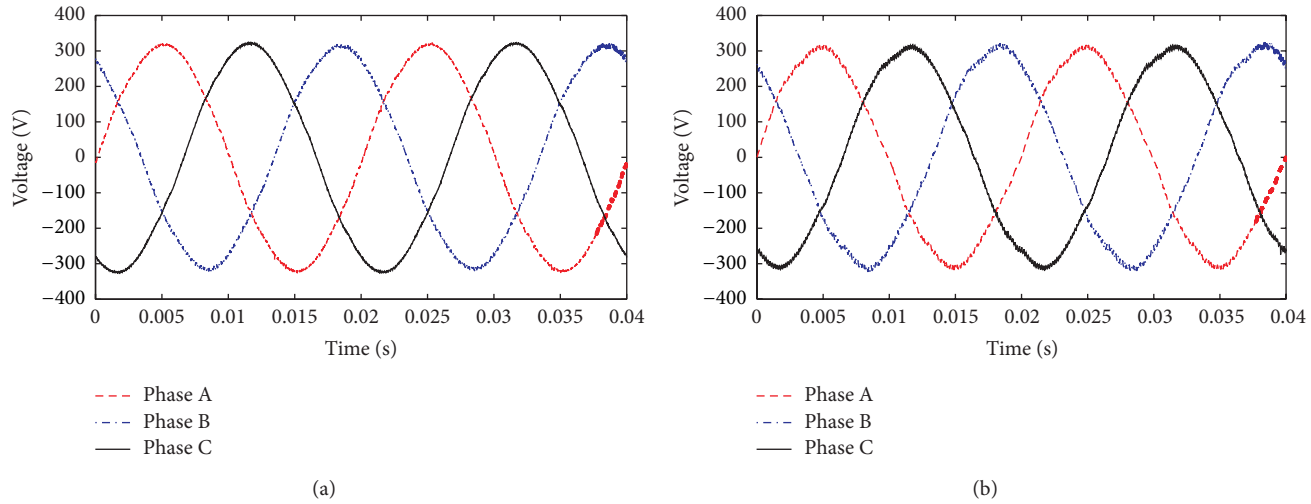

Figure 10: Phase voltages across the load at nominal power from the experimental setup. (a) The voltage with the lowest THD. (b) The voltage with the highest THD.

which is a standard that is followed by most grid connection systems. This shows that the presented grid connection topology is a viable alternative to the more conventional grid connection system from a harmonic distortion perspective. The presented system shows promise with the lowest distortion at the highest power. Together with the overall simplicity of the system, it could be a more cost efficient and robust alternative for grid connection of renewable energy.

7. Conclusions

In this paper, the results from experiments on a tap transformer based grid connection topology are presented. The study evaluates the total harmonic distortion and total demand distortion of the proposed system. From the results, we can see that the system has a TDD and THD below 5% for the full operating range of the turbine. The system THD is lowest at high wind speeds and increases somewhat at lower wind speeds. The TDD of the system has the opposite trend, with low TDD at low wind speeds and an increase as the wind speed increases. A common behavior for both the TDD and THD is that a tap change to a tap with lower step-up ratio results in a lower distortion for the same output power. Furthermore, from the case study we conclude that the magnetization of the transformer gives rise to low order harmonics. If the transformer magnetization during grid connection is supplied by the inverter, some of the low order harmonics in the current might be reduced. This would improve overall system performance.

Acknowledgments

The Swedish Energy Agency and Vinnova are acknowledged for supporting the Swedish Center for Renewable Electric Energy Conversion. This work was conducted within the STandUp for ENERGY strategic research framework.

References

[1] A. D. Hansen and L. H. Hansen, "Wind turbine concept market penetration over 10 years (1995–2004)," *Wind Energy*, vol. 10, no. 1, pp. 81–97, 2007.

[2] J. M. Carrasco, L. G. Franquelo, J. T. Bialasiewicz et al., "Power-electronic systems for the grid integration of renewable energy sources: a survey," *IEEE Transactions on Industrial Electronics*, vol. 53, no. 4, pp. 1002–1016, 2006.

[3] F. Blaabjerg, R. Teodorescu, M. Liserre, and A. V. Timbus, "Overview of control and grid synchronization for distributed power generation systems," *IEEE Transactions on Industrial Electronics*, vol. 53, no. 5, pp. 1398–1409, 2006.

[4] M. Singh, V. Khadkikar, and A. Chandra, "Grid synchronisation with harmonics and reactive power compensation capability of a permanent magnet synchronous generator-based variable speed wind energy conversion system," *IET Power Electronics*, vol. 4, no. 1, pp. 122–130, 2011.

[5] Z. Chen and E. Spooner, "Grid power quality with variable speed wind turbines," *IEEE Transactions on Energy Conversion*, vol. 16, no. 2, pp. 148–154, 2001.

[6] A. D. Hansen, P. Sørensen, L. Janosi, and J. Bech, "Wind farm modelling for power quality," in *27th Annual Conference of the*

IEEE Industrial Electronics Society IECON'2001, pp. 1959–1964, usa, December 2001.

[7] H. Li and Z. Chen, "Overview of different wind generator systems and their comparisons," *IET Renewable Power Generation*, vol. 2, no. 2, pp. 123–138, 2008.

[8] L. H. Hansen, L. Helle, and F. Blaabjerg, *Risø-R-1205(En) Conceptual survey of generators and power electronics for Wind turbines*, 2001.

[9] S. Eriksson, A. Solum, M. Leijon, and H. Bernhoff, "Simulations and experiments on a 12 kW direct driven PM synchronous generator for wind power," *Renewable Energy*, vol. 33, no. 4, pp. 674–681, 2008.

[10] A. Solum, P. Deglaire, S. Eriksson, M. Stålberg, M. Leijon, and H. Bernhoff, "Design of a 12 kw vertical axis wind turbine equipped with a direct driven pm synchronous generator," in *Proceedings of the European Wind Energy Conference & Exhibition (EWEC '06)*, Athen, Greece, February 2006.

[11] P. Deglaire, S. Eriksson, J. Kjellin, and H. Bernhoff, "Experimental results from a 12 kw vertical axis wind turbine with a direct driven pm synchronous generator," in *Proceedings of the European Wind Energy Conference & Exhibition (EWEC '07)*, Milan, Italy, May 2007.

[12] J. Kjellin, F. Bülow, S. Eriksson, P. Deglaire, M. Leijon, and H. Bernhoff, "Power coefficient measurement on a 12 kW straight bladed vertical axis wind turbine," *Renewable Energy*, vol. 36, no. 11, pp. 3050–3053, 2011.

[13] S. Eriksson, H. Bernhoff, and M. Leijon, "FEM simulations and experiments of different loading conditions for a 12 kW direct driven PM synchronous generator for wind power," *International Journal of Emerging Electric Power Systems*, vol. 10, no. 1, article 3, 2009.

[14] I. S. 519-1992, "IEEE recommended practices and requirements for harmonic control in electric power systems," 1993.

[15] T. C. Y. Wang, Z. Ye, G. Sinha, and X. Yuan, "Output filter design for a grid-interconnected three-phase inverter," in *Proceedings of the IEEE 34th Annual Power Electronics Specialists Conference*, vol. 2, pp. 779–784, June 2003.

[16] F. Liu, X. Zha, Y. Zhou, and S. Duan, "Design and research on parameter of LCL filter in three-phase grid-connected inverter," in *Proceedings of the IEEE 6th International Power Electronics and Motion Control Conference (IPEMC '09)*, pp. 2174–2177, Wuhan, China, May 2009.

[17] S. A. Khajehoddin, M. Karimi-Ghartemani, P. K. Jain, and A. Bakhshai, "A control design approach for three-phase grid-connected renewable energy resources," *IEEE Transactions on Sustainable Energy*, vol. 2, no. 4, pp. 423–432, 2011.

[18] B.-G. Cho, S.-K. Sul, H. Yoo, and S.-M. Lee, "LCL filter design and control for grid-connected PWM converter," in *Proceedings of the 8th International Conference on Power Electronics—ECCE Asia: "Green World with Power Electronics" (ICPE ECCE '11)*, pp. 756–763, June 2011.

[19] E. Twining and D. G. Holmes, "Grid current regulation of a three-phase voltage source inverter with an LCL input filter," *IEEE Transactions on Power Electronics*, vol. 18, no. 3, pp. 888–895, 2003.

[20] S. Apelfröjd, F. Bülow, J. Kjellin, and S. Eriksson, "Laboratory verification of system for grid connection of a 12 kw variable speed wind turbine with a permanent magnet synchronous generator," in *Proceedings of European Wind Energy Conference & Exhibition (EWEA '12)*, pp. 16–19, DK, Copenhagen, Denmark, April 2012.

[21] S. Casoria, G. Sybille, and P. Brunelle, "Hysteresis modeling in the MATLAB/Power System Blockset," *Mathematics and Computers in Simulation*, vol. 63, no. 3–5, pp. 237–248, 2003.

[22] J. G. Frame, N. Mohan, and T.-H. Lui, "Hysteresis modeling in an electro-magnetic transients program," *IEEE transactions on power apparatus and systems*, vol. 101, no. 9, pp. 3403–3412, 1982.